



9 **Abstract.** Drifting snow storm is an important aeolian process that reshapes alpine  
10 glaciers and polar ice shelves, and it may also affect the climate system and  
11 hydrological cycle since flying snow particles exchange considerable mass and energy  
12 with air flow. Prior studies have rarely considered the full-scale drifting snow storm in  
13 the turbulent boundary layer, thus, the transportation feature of snow flow higher in  
14 the air and its contribution are largely unknown. In this study, a large eddy simulation  
15 is combined with a subgrid scale velocity model to simulate the atmospheric turbulent  
16 boundary layer, and a Lagrangian particle tracking method is adopted to track the  
17 trajectories of snow particles. A drifting snow storm that is hundreds of meters in  
18 depth and exhibits obvious spatial structures is produced. The snow transport flux  
19 profile at high altitude, previously not observed, is quite different from that near the  
20 surface, thus, the extrapolated transport flux profile may largely underestimate the  
21 total transport flux. At the same time, the development of a drifting snow storm  
22 involves three typical stages, the rapid growth, the gentle growth and the equilibrium  
23 stages, in which the large-scale updrafts and subgrid scale fluctuating velocities  
24 basically dominate the first and second stage, respectively. This research provides an  
25 effective way to get an insight into natural drifting snow storms.

## 26 **1 Introduction**

27 Snow, one type of solid precipitation, is an important sources of material to mountain  
28 glaciers and polar ice sheets, which are widespread throughout high and cold regions  
29 (Chang et al., 2016; Gordon and Taylor, 2009; Lehning et al., 2008). A common  
30 natural phenomenon over snow cover is the drifting snow storm, which occurs when  
31 the wind speed exceeds a critical value (Doorschot et al., 2004; Li and Pomeroy, 1997;  
32 Sturm and Stuefer, 2013). Drifting snow can entrain loose snow particles on the bed  
33 into the air, which may be further transported to high altitude by turbulent eddies  
34 (King, 1990; Mann et al., 2000; Nemoto and Nishimura, 2004). Drifting snow clouds  
35 typically can range in thickness from tens to thousands of meters (Mahesh et al., 2003;  
36 Palm et al., 2011), which may not only affect people's daily life by reducing the  
37 visibility and producing local accumulation (Gordon and Taylor, 2009; Mohamed et  
38 al., 1998), but also can influence the global climate system evolution by changing the  
39 mass and energy balance of ice shelves (Cess and Yagai, 1991; Hanesiak and Wang,  
40 2005; Hinzman et al., 2005; Lenaerts and Broeke, 2012).

41 Several field experiments on drifting snow storm have been performed (Bintanja,  
42 2001; Budd, 1966; Dingle and Radok, 1961; Doorschot et al., 2004; Gallée et al.,  
43 2013; Gordon and Taylor, 2009; Guyomarch et al., 2014; Kobayashi, 1978; Mann et  
44 al., 2000; K Nishimura and Nemoto, 2005; Kouichi Nishimura et al., 2015; J. W.  
45 Pomeroy and Gray, 1990; Sbuhei, 1985; Schmidt, 1982; Sturm and Stuefer, 2013)  
46 since the middle of the last century. However, the measurements are commonly  
47 conducted near the surface, thus, the drifting snow features at high altitude are

48 unknown, and the impacts of these features are difficult to assess. A thorough  
49 investigation documenting the evolution process and structure of a full-scale drifting  
50 snow storm is essential to understand this natural phenomenon and assess its impacts.

51 Drifting snow models, on the other hand, offer a panoramic view of the evolution  
52 process of drifting snow and thus have become one of the most useful research  
53 approaches. Many continuum medium models of drifting snow (Bintanja, 2000; Déry  
54 and Yau, 1999; Schneiderbauer and Prokop, 2011; Uematsu et al., 1991; Vionnet et al.,  
55 2013) have advanced the knowledge of natural drifting snow to a great extent.  
56 However, a particle-tracking drifting snow model is still needed since the particle  
57 characteristics and its motion require further investigation. Although a series of  
58 particle tracking models (Huang et al., 2016; Huang and Shi, 2017; Huang and Wang,  
59 2015; 2016; Nemoto and Nishimura, 2004; Zhang and Huang, 2008; Zwaafink et al.,  
60 2014) have been established, these models have generally focused on the grain-bed  
61 interactions and particle motions near the surface. Thus, a drifting snow model aimed  
62 at producing a large-scale drifting snow storm in a turbulent boundary layer deserves  
63 further exploration.

64 In this study, a drifting snow model in the atmospheric boundary layer that focuses  
65 on the full-scale drifting snow storm is established. The wind field is solved using a  
66 large eddy simulation for the purpose of generating a turbulent atmospheric boundary  
67 layer. A subgrid scale (SGS) velocity is also considered to include the diffusive effect  
68 of small scale turbulence. Finally, particle motion is calculated using a Lagrangian  
69 particle tracking method. The large-scale drifting snow storm is produced under the

70 actions of large-scale turbulent structures combined with a steady-state snow saltation  
 71 boundary condition for particles, and its spatial structures and transport features are  
 72 analyzed.

## 73 **2 Model and methods**

### 74 **2.1 Simulation of a turbulent atmospheric boundary layer**

75 The mesoscale atmosphere prediction pattern ARPS (Advanced Regional Prediction  
 76 System, version 5.3.3) is adopted to simulate the turbulent atmospheric boundary  
 77 layer, in which the filtered three-dimensional compressible non-hydrostatic  
 78 Naiver-Stokes equation is solved (Xue et al., 2001):

$$79 \quad \frac{\partial \rho}{\partial t} + \frac{\partial}{\partial x_i} (\rho \tilde{u}_i) = 0 \quad (1)$$

$$80 \quad \frac{\partial \rho \tilde{u}_i}{\partial t} + \frac{\partial \rho u_i \tilde{u}_j}{\partial x_j} = -\frac{\partial \tilde{p}^*}{\partial x_i} + B \delta_{i3} - \frac{\partial \tau_{ij}}{\partial x_j} \quad (2)$$

81 where ‘ $\sim$ ’ represents variables that are filtered and the filtering scale is  
 82  $\tilde{\Delta} = (\Delta x_1 \Delta x_2 \Delta x_3)^{1/3}$ , in which  $\Delta x_i$  is the grid spacing along streamwise ( $i=1$ ),  
 83 spanwise ( $i=2$ ) and vertical direction ( $i=3$ ), respectively.

84  $\rho = p(1 - q_v / (\varepsilon + q_v))(1 + q_v) / (R_d T)$  is the air density, in which  $p$ ,  $q_v$ ,  $R$  and  $T$  are  
 85 the pressure, the specific humidity, the gas constant ( $287.0 \text{ J kg}^{-1} \text{ K}^{-1}$ ) and  
 86 temperature of the air, respectively, and  $\varepsilon=0.622$  is a constant.  $u_i$  is the  
 87 instantaneous wind speed component, and  $x_i$  is the position coordinate.  $t$  is time,  
 88  $\delta_{ij}$  is the Kronecker delta,  $B = -g \rho' / \rho$  is the buoyancy caused by the air density  
 89 perturbation  $\rho'$ , and  $g$  is the acceleration due to gravity.  $p^* = p' - \alpha \nabla \cdot (\rho \mathbf{u})$  contains  
 90 the pressure perturbation term and damping term, where  $\alpha = 0.5$  is the damping

91 coefficient and  $\nabla$  is the divergence. The subgrid stress  $\tau_{ij}$  can be expressed as  
 92 (Smagorinsky, 1963):

$$93 \quad \tau_{ij} = -2\nu_t \tilde{S}_{ij} = -2(C_s \tilde{\Delta})^2 |\tilde{S}| \tilde{S}_{ij} \quad (3)$$

94 where  $\tilde{S}_{ij} = 0.5(\partial \tilde{u}_i / \partial x_j + \partial \tilde{u}_j / \partial x_i)$  is the strain rate tensor and  $|\tilde{S}| = \sqrt{2\tilde{S}_{ij}\tilde{S}_{ij}}$ ,  $C_s$   
 95 is Smagorinsky coefficient that is determined locally by the dynamic Lagrangian  
 96 model (Meneveau et al., 1996).

## 97 **2.2 Governing equation of particle motion**

98 The trajectory of each snow particle is calculated using a Lagrangian particle tracking  
 99 method. Since a snow particle has is almost  $10^3$  times more dense than air, airborne  
 100 particles are assumed to process only gravity and fluid drag forces, and the governing  
 101 equations of particle motion can be expressed as (Dupont et al., 2013; Huang and  
 102 Wang, 2016; Vinkovic et al., 2006):

$$103 \quad \frac{dx_{pi}}{dt} = u_{pi} \quad (4)$$

$$104 \quad \frac{du_{pi}}{dt} = m_p \frac{V_r}{T_p} f(Re_p) + \delta_{i3} g \quad (5)$$

105 where  $x_{pi}$  and  $u_{pi}$  are the position coordinate and velocity of the snow particle,  
 106 respectively.  $m_p$  is the mass of the solid particle,  $V_r$  is the relative speed between  
 107 the snow particle and air, and  $T_p = \rho_p d_p^2 / 18\rho\nu$  is the particle relaxation time, where  
 108  $\rho_p$  is the particle density ( $900 \text{ kgm}^{-3}$ ),  $d_p$  is the particle diameter and  $\nu = 1.5e-5$   
 109 is the dynamic viscosity of air.  $f(Re_p)$  can be expressed as (Clift et al., 1978):

$$110 \quad f(Re_p) = \begin{cases} 1 & (Re_p < 1) \\ 1 + 0.15 Re_p^{0.687} & (Re_p \geq 1) \end{cases} \quad (6)$$

111 where  $Re_p = V_r d / \nu$  is the particle Reynolds number.

112 Considering the large grid spacing in simulating an atmospheric boundary layer  
 113 (where the information about turbulent vortices smaller than the grid size is missing),  
 114 the SGS velocity is also included and attached on the particle. Namely, the local  
 115 relative is expressed as  $V_{ri} = \tilde{u}_i(x_p) - u_{pi} + u'_i$ , in which  $\tilde{u}_i(\bar{x}_p)$  is the resolved  
 116 large-scale wind speed at the particle's position and is determined by the resolved  
 117 wind speeds of surrounding grid points through the linear interpolation algorithm. The  
 118 SGS velocity can be calculated from the SGS stochastic model of Vinkovic et al.  
 119 (2006):

$$120 \quad du'_i = \left( -\frac{1}{T_L} + \frac{1}{2\tilde{k}} \frac{d\tilde{k}}{dt} \right) u'_i dt + \sqrt{\frac{4\tilde{k}}{3T_L}} d\eta_i(t) \quad (7)$$

121 where  $T_L = 4\tilde{k} / (3C_0\tilde{\varepsilon})$  is the Lagrangian correlation time scale. Here,  $C_0 = 2.1$  is  
 122 the Lagrangian constant,  $\tilde{\varepsilon} = C_\varepsilon \tilde{k}^{3/2} / \tilde{\Delta}$  is the subgrid turbulence dissipation rate,  
 123  $C_\varepsilon = 0.41$  is a constant, and  $d\eta_i$  is the increment of a vector-valued Wiener process  
 124 with zero mean and variance  $dt$ .  $\tilde{k}$  is the subgrid turbulent kinetic energy and can  
 125 be obtained from the transport equation (Deardorff, 1980):

$$126 \quad \frac{\partial \tilde{k}}{\partial t} + \tilde{u}_j \frac{\partial \tilde{k}}{\partial x_j} = \frac{v_t}{3} \frac{g}{\theta_0} \frac{\partial \tilde{\theta}}{\partial x_3} + 2v_t \tilde{S}_{ij}^2 + 2 \frac{\partial}{\partial x_j} \left( v_t \frac{\partial \tilde{k}}{\partial x_j} \right) + \tilde{\varepsilon} \quad (8)$$

127 **2.3** where  $\theta$  is the potential temperature and  $\theta_0$  is the surface potential  
 128 temperature. **Initial conditions of snow particles**

129 To generate a large-scale drifting snow storm, a steady-state snow saltation condition  
 130 is set as the bottom boundary condition for particles. During drifting snow events, the  
 131 sum of residual fluid shear stress  $\tau_f$  and particle-borne shear stress  $\tau_p$  should be

132 equal to the total shear stress  $\tau$ , thus, the particle-borne stress can be expressed as:

$$133 \quad \tau_p = \tau - \tau_f \quad (9)$$

134 Here, the residual fluid shear stress  $\tau_f$  is set to be the threshold shear stress  $\tau_{yf}$   
 135 of drifting snow, which can be read as (Clifton et al., 2006):

$$136 \quad \tau_{yf} = A^2 g d (\rho_p - \rho) \quad (10)$$

137 in which  $A=0.2$  is a constant,  $g$  is the gravity acceleration and  $d$  is the mean  
 138 diameter of the snow particles.

139 At the same time, the particle-borne shear stress at the surface can be calculated  
 140 from the particle trajectories as (Nemoto and Nishimura, 2004):

$$141 \quad \tau_p = \sum_{i=1}^{n_{\downarrow}} m_i u_{pi\downarrow} - \sum_{i=1}^{n_{\uparrow}} m_i u_{pi\uparrow} \quad (11)$$

142 where  $m_i$  is the mass of particle and  $u_{pi\downarrow}$  and  $u_{pi\uparrow}$  are the horizontal speeds of  
 143 impact and lift-off particles, respectively.  $n_{\downarrow}$  and  $n_{\uparrow}$  are the particle number per  
 144 unit area in unit time of impact and lift-off grains, respectively, which should be  
 145 equivalent in steady-state saltation. Thus, the number of lift-off particles per unit area  
 146 is:

$$147 \quad n_{\uparrow} = n_{\downarrow} = \frac{\tau_p}{\langle m_i \rangle (1 - \langle e_h \rangle) \langle u_{pi\downarrow} \rangle} \quad (12)$$

148 in which  $\langle \rangle$  indicates the overall average, and  $e_h$  is the horizontal restitution  
 149 coefficient of snow particle. According to Sugiura and Maeno (2000), the mean  
 150 horizontal restitution coefficient can be expressed as:

$$151 \quad \langle e_h \rangle = \begin{cases} 0.48 \theta_i^{0.01} & v_i \leq 1.27 \text{ms}^{-1} \\ 0.48 \left( \frac{v_i}{1.27} \right)^{-\log\left(\frac{v_i}{1.27}\right)} \theta_i^{0.01} & v_i > 1.27 \text{ms}^{-1} \end{cases} \quad (13)$$



152 where  $\theta_i$  and  $v_i$  are the impact velocity and angle, respectively. Here,  $\theta_i$  has a  
 153 mean value of approximately  $10^\circ$  (Sugiura and Maeno, 2000), and  $\langle v_i \rangle$  is set to be  
 154 the threshold of impact velocity. Considering the steady-state saltation condition (one  
 155 impact particle generates one ejecta on average),  $\langle v_i \rangle$  is determined by setting  
 156 ejection number  $n_e = 0.51v_i^{0.6}\theta_i^{0.16}$  equal to 1. In this way, the mean horizontal  
 157 velocity of impact particles can be obtained through  $\langle u_{pi\downarrow} \rangle = \langle v_i \rangle \cos \langle \theta_i \rangle$ .

158 Then, the velocities of lift-off particles can be obtained from the restitution  
 159 coefficient of snow. The horizontal restitution coefficient obeys the normal  
 160 distribution with a mean value given in Eq. 13, and a standard variance as follow  
 161 (Sugiura and Maeno, 2000):

$$162 \quad \sigma^2 = \begin{cases} 0.07\theta_i^{-0.06} & v_i \leq 0.52 \text{ ms}^{-1} \\ 0.07\left(\frac{v_i}{0.52}\right)^{-\log\left(\frac{v_i}{0.52}\right)}\theta_i^{-0.06} & v_i > 0.52 \text{ ms}^{-1} \end{cases} \quad (14)$$

163 On the other hand, the vertical restitution coefficient can be described by a two  
 164 parameter gamma function (see Eq. 17), in which the parameter  $\alpha$  and  $\beta$  can be  
 165 expressed as (Sugiura and Maeno, 2000):

$$166 \quad \alpha = \begin{cases} 1.22\theta_i^{0.47} & v_i \geq 0.84 \text{ ms}^{-1} \\ 1.22\left(\frac{v_i}{0.84}\right)^{\log\left(\frac{v_i}{0.84}\right)}\theta_i^{0.47} & 0.84 < v_i \leq 1.23 \text{ ms}^{-1} \\ 1.22\left(\frac{v_i}{0.84}\right)^{\log\left(\frac{v_i}{0.84}\right)}\left(\frac{v_i}{1.23}\right)^{-2\log\left(\frac{v_i}{1.23}\right)}\theta_i^{0.47} & v_i \geq 1.23 \text{ ms}^{-1} \end{cases} \quad (15)$$

$$167 \quad \beta = \begin{cases} 12.85\theta_i^{-1.41} & v_i \geq 0.84 \text{ ms}^{-1} \\ 12.85\left(\frac{v_i}{0.84}\right)^{-\log\left(\frac{v_i}{0.84}\right)}\theta_i^{-1.41} & 0.84 < v_i \leq 1.23 \text{ ms}^{-1} \\ 12.85\left(\frac{v_i}{0.84}\right)^{-\log\left(\frac{v_i}{0.84}\right)}\left(\frac{v_i}{1.23}\right)^{\log\left(\frac{v_i}{1.23}\right)}\theta_i^{-1.41} & v_i \geq 1.23 \text{ ms}^{-1} \end{cases} \quad (16)$$

168 In this condition, if some of the snow particles within the saltation layer are  
169 transported to higher in the air by turbulent vortexes (the saltation layer becomes  
170 undersaturated), more particles will lift-off from the surface to replenish the saltation  
171 layer until a saturated state is reached.

## 172 **2.4 Simulation details**

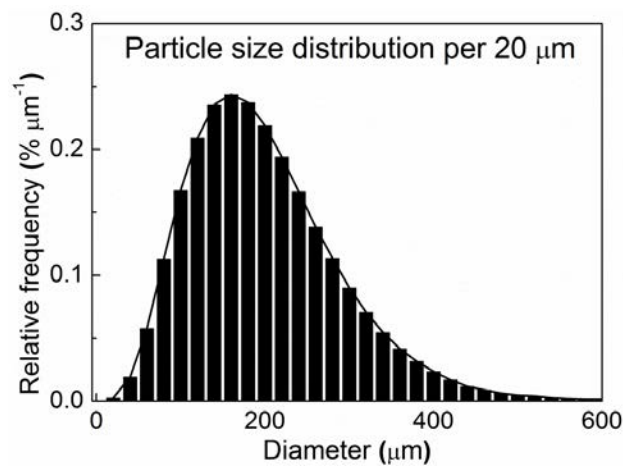
173 The computational domain is  $1000 \times 500 \times 1000$  m, with a uniform horizontal grid  
174 size of 5 m adopted to solve finer vortex structure in the atmospheric boundary layer.

175 The mean grid size in the vertical direction is 20 m, with a grid refinement algorithm  
176 adopted near the surface (the finest grid size is 1 m). Periodic boundaries are used  
177 along streamwise and spanwise dimensions, and the bottom is set as a grid wall. The  
178 top is set as an open radiation boundary with a Rayleigh damping layer that is 250 m  
179 in depth.

180 The atmosphere is neutral with an initial potential temperature of 300K, and an  
181 initial relative humidity of 90%. The initial wind profile is logarithmic with a surface  
182 roughness of 0.1m (Doorschot et al., 2004). Atmospheric turbulence is induced by  
183 random initial potential temperature perturbations at the first-level grid level with a  
184 maximum magnitude of 0.5K, and is sustained by a constant heat flux at the bottom.  
185 The constant heat flux is  $50 \text{ Wm}^{-2}$  according to the observation of Pomeroy and  
186 Essery (1999). And the evolution time for a turbulent boundary layer is 5 times of the  
187 large-eddy turnover time  $t_*$  ( $\equiv H/u_*$ , where  $H$  is the boundary layer depth and  $u_*$   
188 is the friction velocity). Actually, this condition corresponds to a ‘intermediate’  
189 turbulent boundary layer that dominated by wind shear force (Moeng and Sullivan,

190 1994). Thus, the structures of the drifting snow storm should not be affected by the  
191 changing surface heat flux significantly if the surface heat flux is small. Further  
192 simulations with different values of surface heat flux ( $<100 \text{ Wm}^{-2}$ ) also prove this  
193 point.

194 For particles, periodic boundary conditions are also used at lateral boundaries, and  
195 a rebound boundary condition without energy loss is adopted at the model top. The  
196 bottom boundary condition for particles is given in Sect. 2.3, and is updated every 0.5  
197 s. Additionally, each particle represents one particle parcel for the purpose of reducing  
198 computational complexity. In this simulation, each particle parcel contains  $10^7$  snow  
199 particles. The large time step and small time step (acoustic wave integral) for the wind  
200 field calculation are 0.1 s and 0.02 s, respectively, and the particle time step is  
201 determined by the minimum of particle relaxation time.



202  
203 **Figure 1.** Size distribution of lift-off snow particles in this simulation.

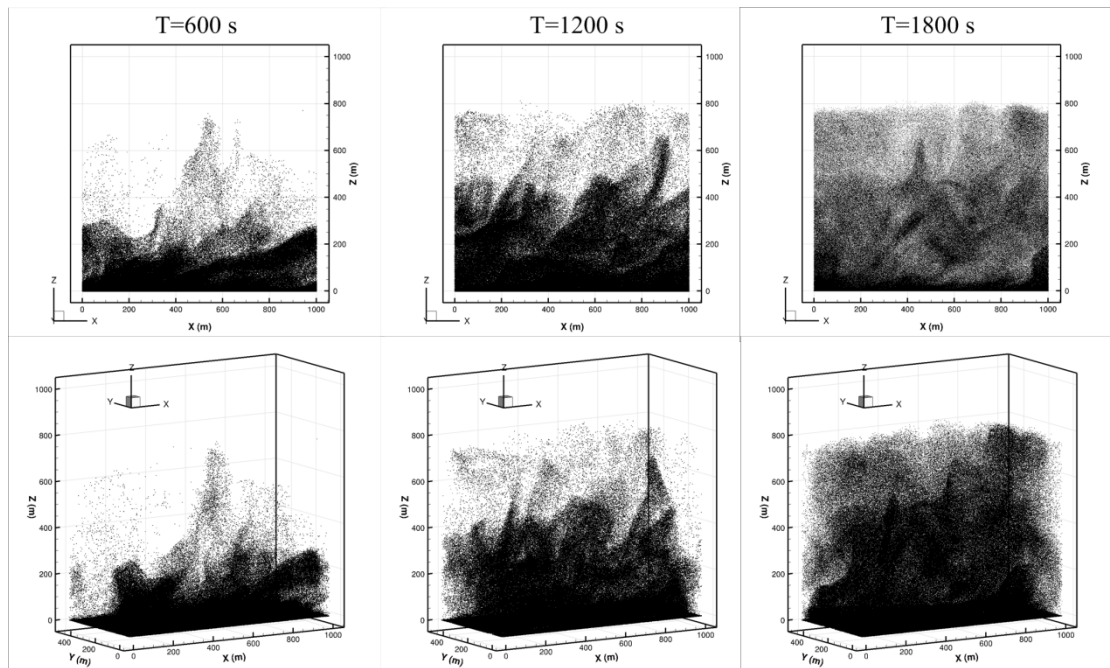
204 The size distribution of lift-off particles in drifting snow can be well described by  
205 the two-parameter gamma function (Budd, 1966; Gordon and Taylor, 2009;  
206 Nishimura and Nemoto, 2005; Schmidt, 1982):

207 
$$f(d) = \frac{d^{\alpha-1}}{\beta^\alpha \Gamma(\alpha)} \exp\left(-\frac{\beta}{d}\right) \quad (17)$$

208 where  $d$  is the particle diameter, and  $\alpha$  and  $\beta$  are the shape and scale parameter of  
 209 the distribution, respectively. In this simulation, the diameters of lift-off snow  
 210 particles are given randomly from a gamma function with the parameters of  $\alpha = 4$   
 211 and  $\beta = 50$ , as shown in Fig. 1, which is also consistent with observed particle size  
 212 distributions (Nishimura and Nemoto, 2005; Schmidt, 1982).

### 213 3 Results and discussions

#### 214 3.1 Model validation

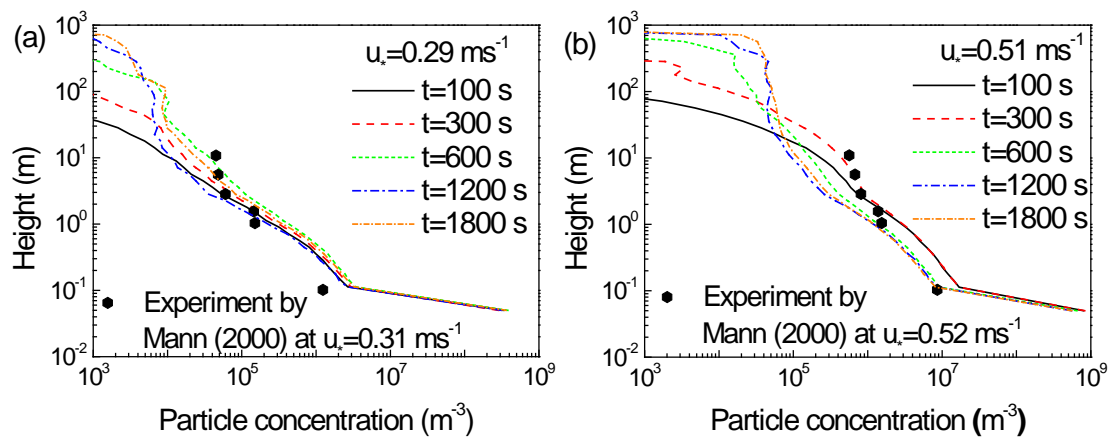


215  
 216 **Figure 2.** Drifting snow storm at different moments under the friction velocity of 0.29  
 217  $\text{ms}^{-1}$ .

218 When drifting snow occurs in the atmospheric boundary layer, updrafts and  
 219 turbulence fluctuations can send snow particles to high altitude, forming a fully  
 220 developed drifting snow storm. Fig. 2 shows the drifting snow storm in the  
 221 atmospheric boundary layer at different moments, in which the friction velocity is

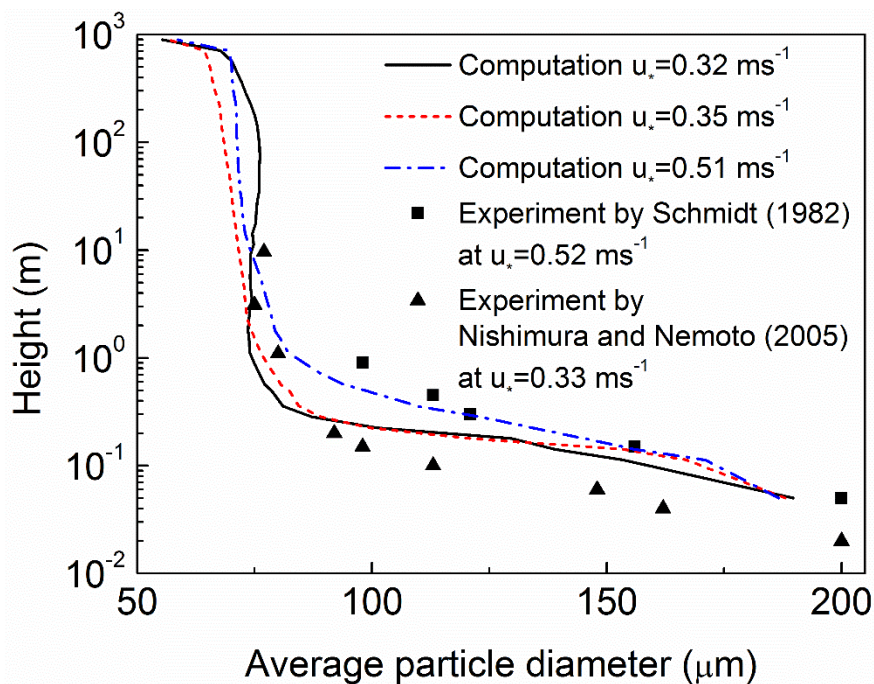
222  $u_* = 0.29 \text{ ms}^{-1}$  and dark spots represent snow particles. It can be seen that drifting  
 223 snow storm experiences an evolution process from near the surface to high altitudes,  
 224 which induces the fact that particle concentration decreases along increasing height.  
 225 The high concentrations of drifting snow cloud are generally below 500 m, though  
 226 snow particles may reach up to approximately 800 m under this condition. This is also  
 227 consistent with observations (Mahesh et al., 2003; Palm et al., 2011).

228 Since a drifting snow storm exhibits a different structure from bottom to top, the  
 229 evolution of particle number density profile in the drifting snow storm is shown in Fig.  
 230 3, which is also compared with measurements of Mann et al. (2000). From this figure,  
 231 the thickness of the drifting snow layer obviously increases with time, and almost  
 232 approaches its steady state after 1200 s. At the same time, the particle number density  
 233 basically decreases with height, which is consistent with the measurements of Mann  
 234 et al. (2000) at various friction velocities. The predicted particle number density at the  
 235 surface is much larger than at higher altitude and observations, mainly because the  
 236 saltating particles are also included.



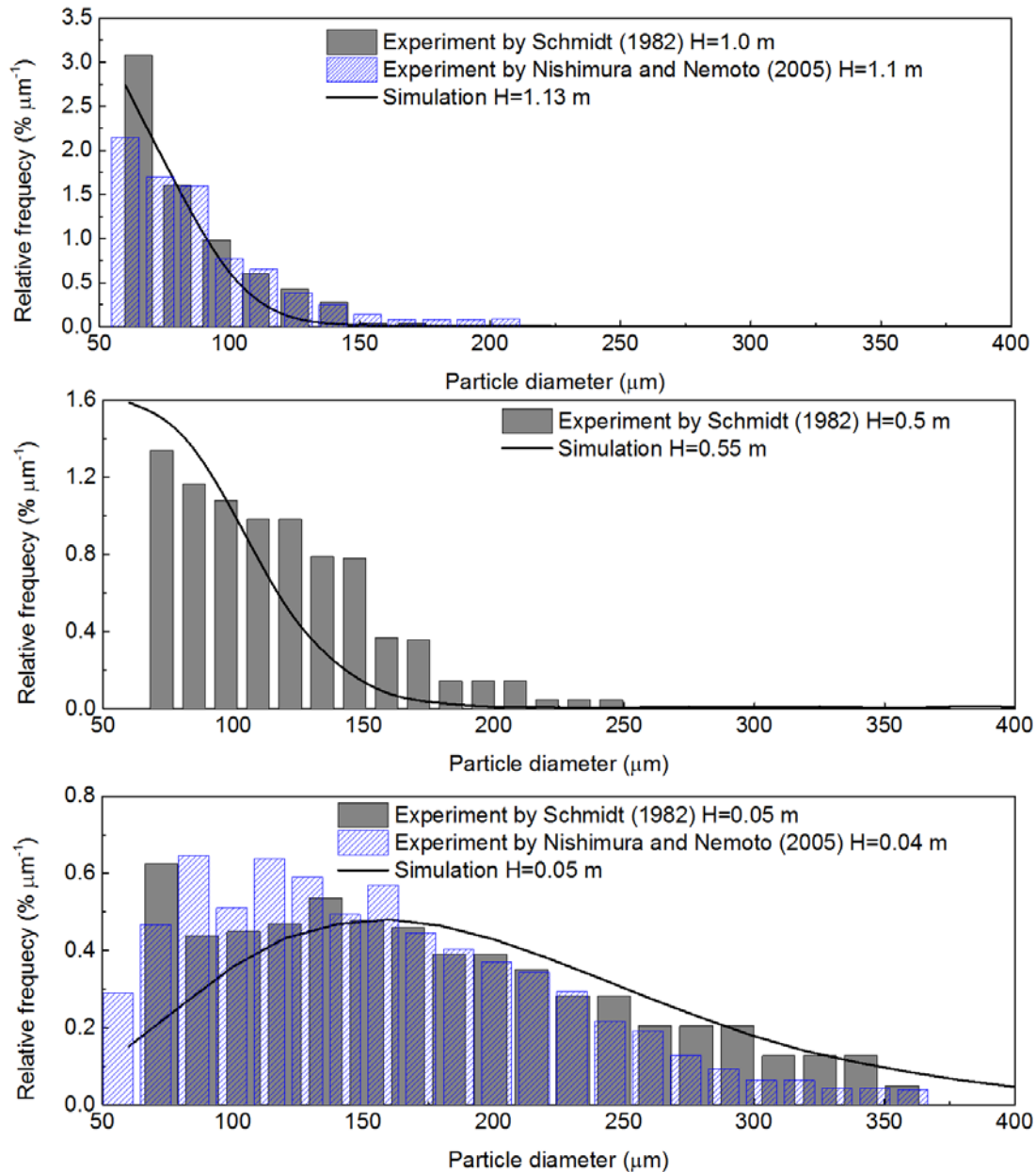
237  
 238 **Figure 3.** Evolution of particle number density under various friction velocities (a)  
 239  $0.29 \text{ ms}^{-1}$  and (b)  $0.51 \text{ ms}^{-1}$ .

240 Generally, smaller particles are more likely to be transported higher in the air. Fig.  
 241 4 shows the variation of modeled average particle diameter versus height, which is  
 242 also compared with various field measurements (Nishimura and Nemoto, 2005;  
 243 Schmidt, 1982). Similar to the field observations, the average particle size basically  
 244 decreases with height at lower altitude but is almost constant above 1 m. The average  
 245 particle diameter is approximately 75  $\mu\text{m}$  ranging from one meter to hundreds of  
 246 meters in height, which is also consistent with the measurements of K Nishimura and  
 247 Nemoto (2005).



248  
 249 **Figure 4.** Variation of average particle diameter versus height.

250 Then, the particle size distributions at various heights are also compared with  
 251 experiment results. As shown in Fig. 5, the heights are 0.05 m, 0.5 m and 1 m. The  
 252 modeled particle size distributions at various heights are consistent with the  
 253 measurements (Nishimura and Nemoto, 2005; Schmidt, 1982). Therefore, the  
 254 established model is able to produce a large-scale drifting snow storm.



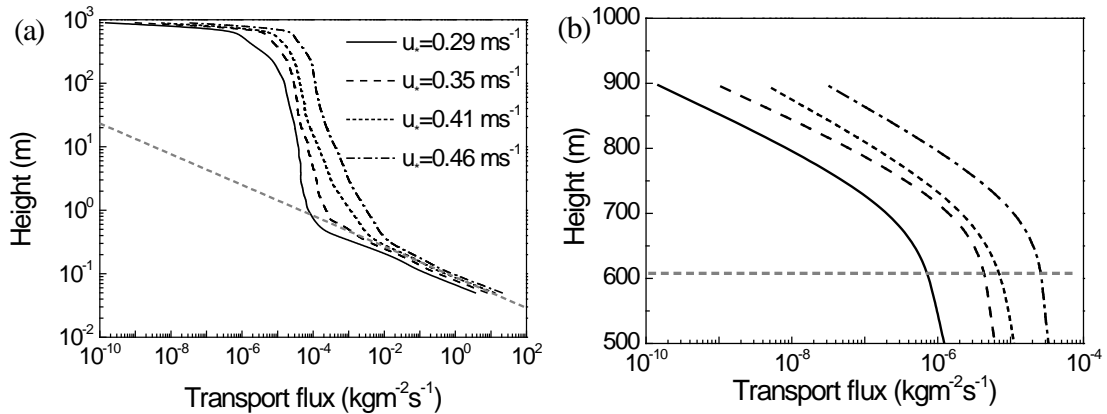
255

256 **Figure 5.** Particle size distribution at various heights.

257 Besides, it can be seen that the proportion of particles below 100  $\mu\text{m}$  in diameter  
 258 at 0.05 m is smaller than that of the experimental result. The reason could be that  
 259 mid-air collisions, occurred frequently within the high concentration saltating snow  
 260 cloud at the near surface, play an important role in conveying larger particles to  
 261 higher altitude(Carneiro et al., 2013). However, the mid-air collision mechanism is  
 262 beyond the scope of the current study.

263 **3.2 Snow transport flux**

264 The snow transport flux is of great importance to predict the mass and energy  
265 balances of ice sheets. The total transport flux can be obtained from vertical  
266 integration of the snow transport flux profile.



267

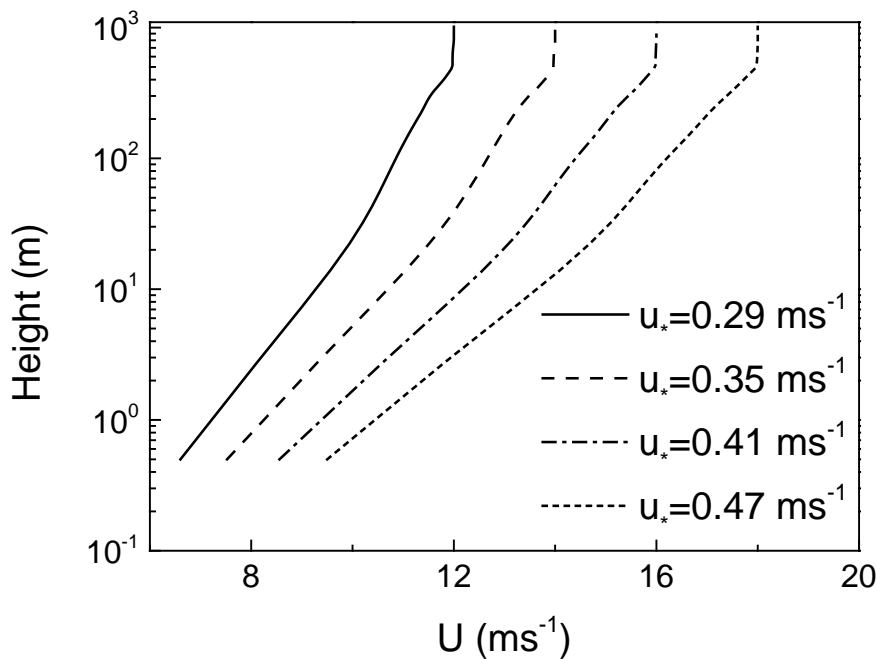
268 **Figure 6.** Variations of snow transport flux versus height.

269 The profiles of snow transport rate, per unit area, per unit time, under various  
270 friction velocities are shown in Fig. 6(a). It can be seen that the transport flux  
271 undergoes a sharp decrease with height at lower altitude (e.g., below 1.0 m), however,  
272 the transport flux tends to decrease rather gentle until almost the top of the drifting  
273 snow storm, as shown in Fig. 6(b), probably due to the large-scale turbulent motion  
274 and increasing wind speed with height. In other words, the suspension flux of drifting  
275 snow at higher altitudes, previously not observed, may be much larger than we  
276 previously thought. The mean horizontal wind speed profiles of the fully developed  
277 turbulent boundary layer under various friction velocities are shown in Fig. 7. The  
278 horizontal wind speed increases with height and changes into a constant above the  
279 boundary layer. The rapid decrease of the snow transport flux occurs at about the top  
280 of the turbulent boundary layer, mainly because turbulences become weaker above



281 this height and less particles can be transported to a higher altitude.

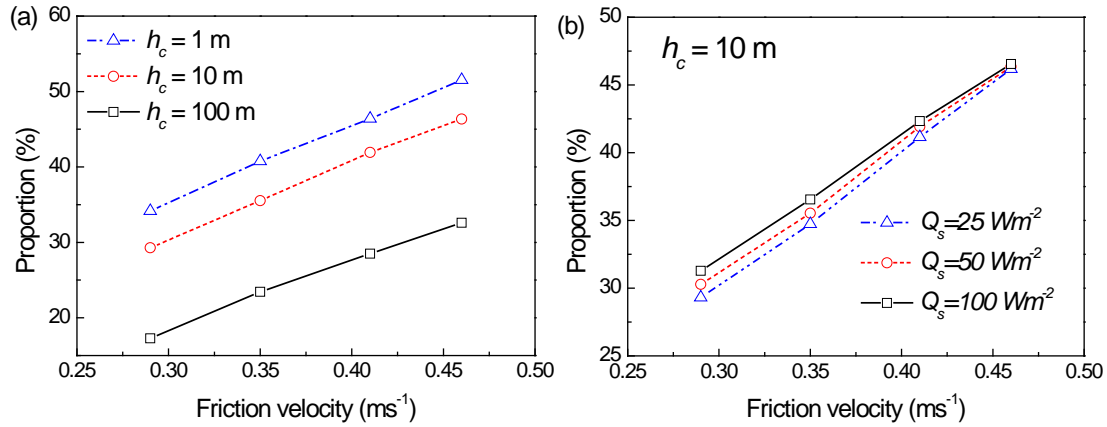
282 Besides, the transition of snow transport flux profile at about 1 m should be  
283 mainly caused by the different motion states of particles with different particle sizes,  
284 as shown in Fig. 4. Above the critical height, particles generally follow the turbulent  
285 flow in the state of suspension because their gravities and relaxation times are small  
286 enough. However, plenty of larger particles at the near surface make the particles  
287 velocity differs from the wind speed, since particle inertia plays an important role.



288  
289 **Figure 7.** Horizontal wind speed profiles of the fully developed turbulent boundary  
290 layer under various friction velocities.

291 In previous studies, only the transport fluxes at the near surface are commonly  
292 measured (Mann et al., 2000; Nishimura and Nemoto, 2005; Schmidt, 1982; 1984;  
293 Tabler, 1990), thus, the features of the entire transport flux profile is largely unclear,  
294 which may result in considerable uncertainties about the total transport flux. The  
295 proportions of suspension flux above a given height  $h_c$  (referred as  $Q_c$ ) to the total

296 suspension flux  $Q_s$  are shown in Fig. 7, in which snow particles below 0.1 m are not  
 297 calculated (Mann et al., 2000).



298  
 299 **Figure 8.** Proportion of suspension flux above  $h_c$  to the total suspension flux under  
 300 (a) various friction velocities and (b) various surface heat fluxes  $Q_s$ .

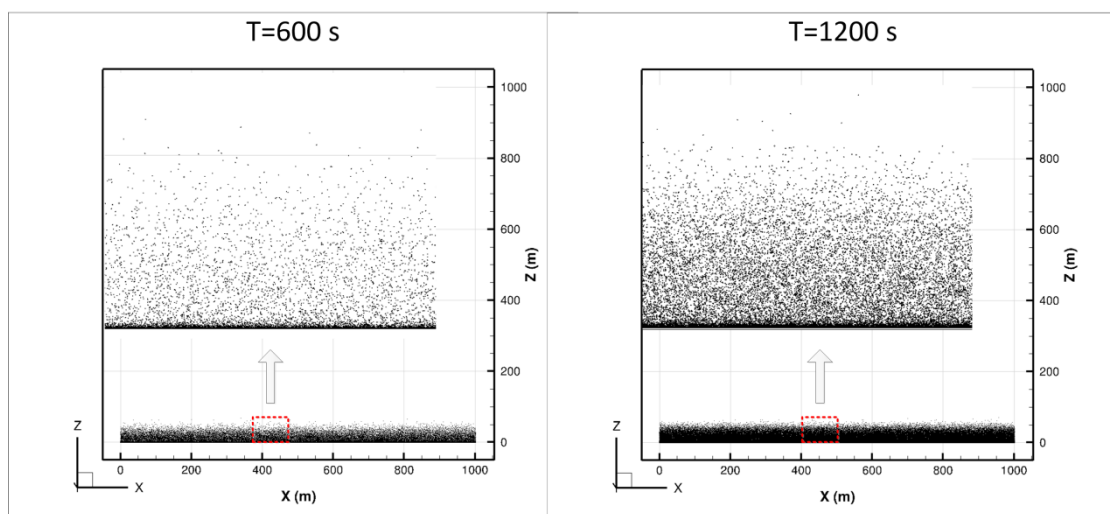
301 From Fig. 8 (a), the contribution of  $Q_c$  to the total suspension flux is  
 302 non-negligible under various  $h_c$ , the proportion of  $Q_c$  when  $h_c=100$  m to the total  
 303 suspension flux has exceeded 30% when the friction velocity is  $0.46 \text{ ms}^{-1}$ . At the same  
 304 time, the proportion of  $Q_c$  to the total suspension flux increases with friction  
 305 velocity but decreases with increasing  $h_c$ . From Fig. 8 (b), it can be seen that the  
 306 proportion  $Q_c$  to the total suspension flux is only slightly affected by the surface  
 307 heat flux, which indicates that the structures of drifting snow storm are not sensitive  
 308 to the surface heat flux under this condition. The influence of surface heat flux is also  
 309 weakened by the increasing friction velocity, mainly because larger friction velocity  
 310 results in stronger turbulence under the actions of wind shear.

311 In this way, not only the snow transport flux, but also the sublimation of  
 312 suspended snow particles should be reevaluated because the sublimation rate of snow  
 313 particles higher in the air may be much larger than near the surface due to the lower

314 air humidity and greater wind speed at higher altitude (Mann et al., 2000; Nishimura  
315 and Nemoto, 2005; Schmidt, 1982; 1984; Tabler, 1990).

### 316 3.3 Structures in a drifting snow storm

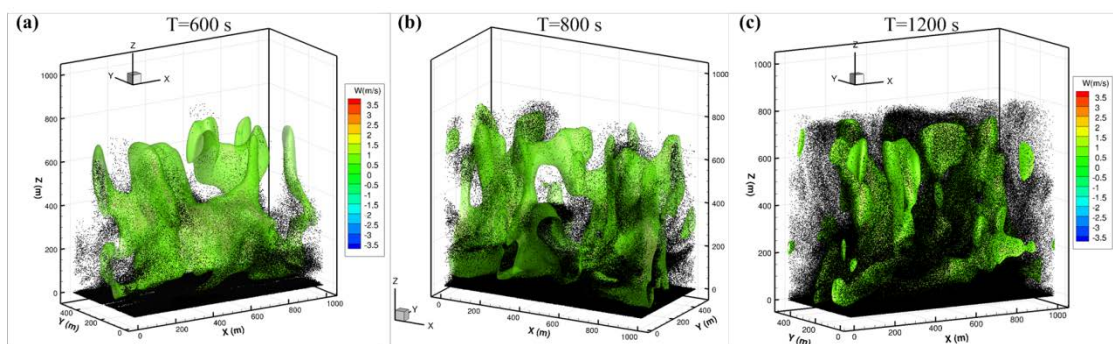
317 In a drifting snow storm, particles aggregate locally and produce special spatial  
318 structures (as shown in Fig. 2). These structures should be directly related to the  
319 turbulence structures present in the atmospheric boundary layer. Drifting snow storms  
320 without atmospheric turbulence are shown in Fig. 9. This simulation is achieved by  
321 replacing the resolved wind speed at particle's position ( $\tilde{u}_i(\vec{x}_p)$ ) with a given value  
322 obtained from the standard logarithmic profile, and the other model settings and  
323 simulation procedures stay the same with other simulations. In this way, the effect of  
324 large-scale turbulent structures on the development of the drifting snow storm  
325 vanishes. Compared with Fig. 2, drifting snow particles mainly travel at the near  
326 surface with a uniform spatial distribution when atmospheric turbulence is not  
327 included.



328

329 **Figure 9.** Drifting snow storm without atmospheric turbulence under friction velocity  
330 of  $0.35 \text{ ms}^{-1}$ .

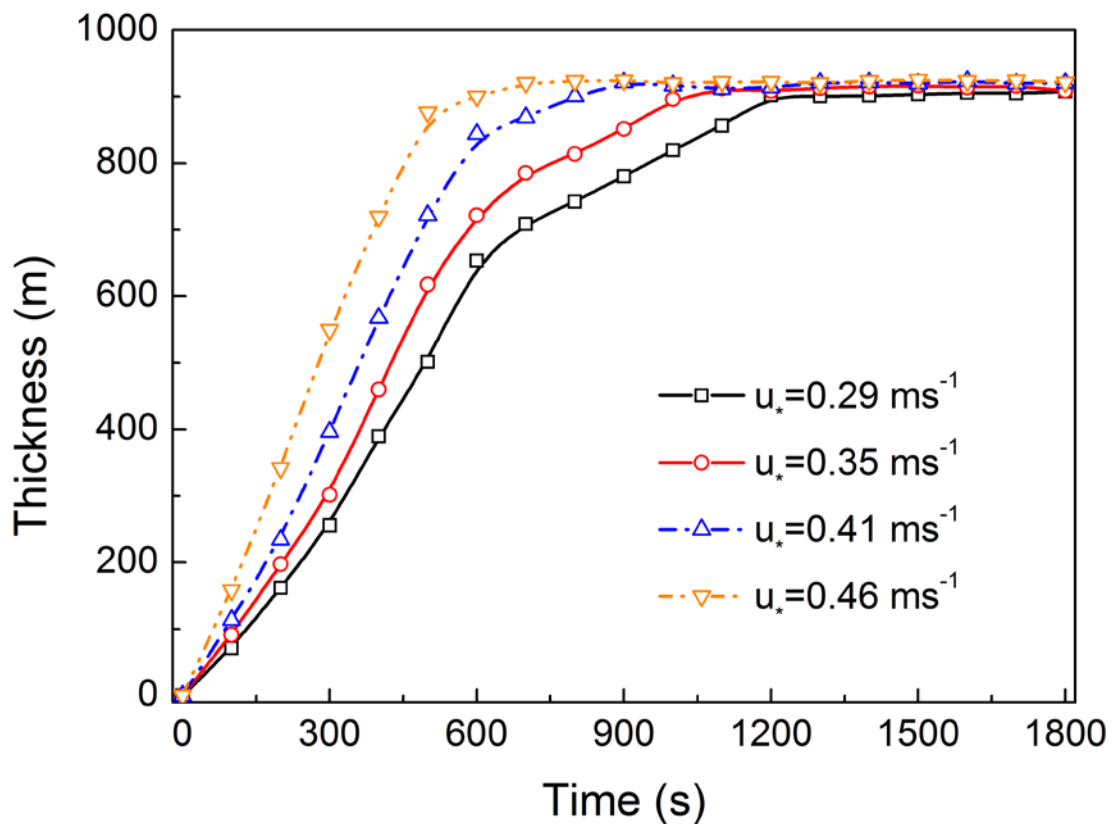
331 It is known that snow particles will become suspended if the local vertical wind  
 332 speed exceeds the terminal velocity of particle. In a turbulent atmospheric boundary  
 333 layer, there exists a large amount of turbulent structures with different scales and  
 334 shapes. The vertical wind speed component of large-scale turbulence (namely, updraft)  
 335 plays an important role in carrying snow particles to high altitude, while small scale  
 336 turbulence (e.g., the SGS fluctuating velocity) tends to spread particles from high  
 337 concentration zones to low concentration zones. As shown in Fig. 10(a), at the initial  
 338 period of a drifting snow storm, the structures in the drifting snow storm are  
 339 consistent with large-scale updrafts, and snow particles are mainly located in the  
 340 updraft. With the further development of the drifting snow storm, as shown in Fig.  
 341 10(b), more snow particles are scattered around the updraft bubbles although high  
 342 concentration particle clouds are still in the wind bubbles. When drifting snow storm  
 343 approaches its saturated state, snow particle clouds are almost connected together with  
 344 numerous high concentration zones inside.



345  
 346 **Figure 10.** Evolution of drifting snow storm and vertical wind speed bubbles under  
 347 friction velocity of  $0.35 \text{ ms}^{-1}$ , and wind bubbles are iso-surface of vertical wind speed  
 348 with a value of  $1.0 \text{ ms}^{-1}$  (corresponding to the critical wind speed at which the particle  
 349 of mean particle size becomes suspended particle, since the maximum diameter of

350 suspended particles is found to be approximately equals to the mean particle size of  
351 the lift-off particles).

352 The evolution of the depth of drifting snow storm can be divided into three typical  
353 stages. In sequence, these phases are the rapid growth phase, the gentle growth stage,  
354 and an equilibrium state, as shown in Fig. 11. Here, the depth of drifting snow storm  
355 refers to the average height of the topmost particle during this period (100 s). The  
356 rapid growth stage is mainly driven by large-scale turbulent motion, while the  
357 turbulent diffusion by the SGS fluctuating velocity is the main contributor to the  
358 gentle growth stage. The duration of second stage decreases with increasing friction  
359 velocity, which mainly comes from the stronger turbulent diffusion under larger  
360 friction velocities.



361

362 **Figure 11.** Time evolutions of the thickness of drifting snow storm under various

363 friction velocities.

364 At the same time, the time required for the drifting snow storm to reach its  
365 maximum thickness decreases with friction velocity, ranging from about 1200 s to  
366 approximate 600 s when the friction velocity increases from  $0.29 \text{ ms}^{-1}$  to  $0.46 \text{ ms}^{-1}$ .  
367 The thicknesses of saturated drifting snow storms are almost constant with a value  
368 approximately 900 m under different friction velocities, probably because the  
369 boundary layer depth as well as the surface heat flux are unchanged. Higher domain  
370 heights are also tested with the same model settings, and the thickness of the drifting  
371 snow seems basically unchanged. Drifting snow storm with difference thicknesses  
372 may be achieved by changing the initial state of the air and surface heat flux. Thus,  
373 the final thickness of a drifting snow storm should be largely dependent on the  
374 maximum height of atmospheric turbulences.

#### 375 **4 Conclusion**

376 In this work, large-scale drifting snow storms are simulated in a large eddy simulation  
377 combined with a particle tracking model that includes subgrid scale velocity  
378 fluctuations. A typical drifting snow storm of several hundred meters in depth is  
379 generated, and the structure of the particle cloud with different concentrations is also  
380 produced. The transport flux profile has obviously different slopes near the surface  
381 compared to higher altitudes, that is, transport flux at near surface decreases with  
382 height sharply, but decreases more gentle at higher altitude. Previous studies may  
383 largely underestimate the total transport during drifting snow storms.

384 At the same time, the evolution of the thickness of drifting snow storm generally

385 contains three stages. Drifting snow storm development generally begins with a rapid  
386 growth stage driven by the large scale atmospheric turbulent motions, followed by a  
387 gentle growth stage driven by the SGS fluctuating wind speed, before reaching an  
388 equilibrium stage when the drifting snow approaches a saturated state. The second  
389 stage becomes shorter with increasing friction velocity, mainly because stronger  
390 turbulence under higher friction velocity enhances the turbulent diffusion of particles.

391

392 *Acknowledgements.* This work is supported by the CARDC Fundamental and Frontier  
393 Technology Research Fund (FFTRF-2017-08, FFTRF-2017-09), the State Key  
394 Program of National Natural Science Foundation of China (91325203), the National  
395 Natural Science Foundation of China (11172118, 41371034), and the Innovative  
396 Research Groups of the National Natural Science Foundation of China (11121202),  
397 National Key Technologies R & D Program of China (2013BAC07B01).

#### 398 **References:**

- 399 Bintanja, R.: Snowdrift suspension and atmospheric turbulence. Part I: Theoretical  
400 background and model description, *Boundary-Layer Meteorology*, 95, 343-368,  
401 2000.
- 402 Bintanja, R.: Characteristics of snowdrift over a bare ice surface in Antarctica, *Journal*  
403 *of Geophysical Research Atmospheres*, 106, 9653-9659, 2001.
- 404 Budd, W. F.: The Byrd snow drift project : outline and basic results, 71-134, *American*  
405 *Geophysical Union*, Washington, DC, 1966.
- 406 Carneiro, M. V., Araújo, N. A., Pähtz, T., and Herrmann, H. J.: Midair collisions  
407 enhance saltation, *Phys.rev.lett*, 111, 058001, 2013.
- 408 Cess, R. D., and Yagai, I.: Interpretation of Snow-Climate Feedback as Produced by  
409 17 General Circulation Models, *Science*, 253, 888-892, 1991.
- 410 Chang, A. T. C., Foster, J. L., and Hall, D. K.: Nimbus-7 SMMR Derived Global  
411 Snow Cover Parameters, *Annals of Glaciology*, 9, 39-44, 2016.
- 412 Clift, R., Grace, J. R., and Weber, M. E.: Bubbles, drops, and particles, 263-264, 1978.
- 413 Clifton, A., Rüedi, J. D., and Lehning, M.: Snow saltation threshold measurements in

414 a drifting-snow wind tunnel, *Journal of Glaciology*, 52, 585-596, 2006.

415 Déry, S. J., and Yau, M. K.: A Bulk Blowing Snow Model, *Boundary-Layer*  
416 *Meteorology*, 93, 237-251, 1999.

417 Deardorff, J. W.: Stratocumulus-capped mixed layers derived from a  
418 three-dimensional model, *Boundary-Layer Meteorology*, 18, 495-527, 1980.

419 Dingle, W. R. J., and Radok, U.: Antarctic snow drift and mass transport, *Int. Assoc.*  
420 *Sci. Hydrol. Publ.*, 55, 77-81, 1961.

421 Doorschot, J. J. J., Lehning, M., and Vrouwe, A.: Field measurements of snow-drift  
422 threshold and mass fluxes, and related model simulations, *Boundary-Layer*  
423 *Meteorology*, 113, 347-368, 2004.

424 Dupont, S., Bergametti, G., Marticorena, B., and Simoëns, S.: Modeling saltation  
425 intermittency, *Journal of Geophysical Research Atmospheres*, 118, 7109-7128,  
426 2013.

427 Gallée, H., Trouvilliez, A., Agosta, C., Genthon, C., Favier, V., and Naaim-Bouvet, F.:  
428 Transport of Snow by the Wind: A Comparison Between Observations in Adélie  
429 Land, Antarctica, and Simulations Made with the Regional Climate Model MAR,  
430 *Boundary-Layer Meteorology*, 146, 133-147, 2013.

431 Gordon, M., and Taylor, P. A.: Measurements of blowing snow, Part I: Particle shape,  
432 size distribution, velocity, and number flux at Churchill, Manitoba, Canada, *Cold*  
433 *Regions Science & Technology*, 55, 63-74, 2009.

434 Guyomarch, G., Goetz, D., Vionnet, V., Naaimbouvet, F., and Deschatres, M.:  
435 Observation of Blowing Snow Events and Associated Avalanche Occurrences,  
436 2014.

437 Hanesiak, J. M., and Wang, X. L.: Adverse-Weather Trends in the Canadian Arctic,  
438 *Journal of Climate*, 18, 3140-3156, 2005.

439 Hinzman, L. D., Bettez, N. D., Bolton, W. R., Chapin, F. S., Dyrgerov, M. B., Fastie,  
440 C. L., Griffith, B., Hollister, R. D., Hope, A., and Huntington, H. P.: Evidence and  
441 Implications of Recent Climate Change in Northern Alaska and Other Arctic  
442 Regions, *Climatic Change*, 72, 251-298, 2005.

443 Huang, N., Dai, X., and Zhang, J.: The impacts of moisture transport on drifting snow  
444 sublimation in the saltation layer, *Atmospheric Chemistry & Physics*, 16,  
445 7523-7529, 2016.

446 Huang, N., and Shi, G.: The significance of vertical moisture diffusion on drifting  
447 Snow sublimation near snow surface, *Cryosphere*, 11, 3011-3021, 2017.

448 Huang, N., and Wang, Z. S.: A 3-D simulation of drifting snow in the turbulent  
449 boundary layer, *Cryosphere Discussions*, 9, 301-331, 2015.

450 Huang, N., and Wang, Z. S.: The formation of snow streamers in the turbulent  
451 atmosphere boundary layer, *Aeolian Research*, 23, 1-10, 2016.

452 King, J. C.: Some measurements of turbulence over an antarctic ice shelf, *Quarterly*  
453 *Journal of the Royal Meteorological Society*, 116, 379-400, 1990.

454 Kobayashi, S.: Snow Transport by Katabatic Winds in Mizuho Camp Area, East  
455 Antarctica, *Journal of the Meteorological Society of Japan*, 56, 130-139, 1978.

456 Lehning, M., Löwe, H., Ryser, M., and Raderschall, N.: Inhomogeneous precipitation  
457 distribution and snow transport in steep terrain, *Water Resources Research*, 44,



458 278-284, 2008.

459 Lenaerts, J. T. M., and Broeke, M. R. V. D.: Modeling drifting snow in Antarctica  
460 with a regional climate model: 2. Results, *Journal of Geophysical Research*  
461 *Atmospheres*, 117, D05109, 2012.

462 Li, L., and Pomeroy, J. W.: Estimates of Threshold Wind Speeds for Snow Transport  
463 Using Meteorological Data, *Journal of Applied Meteorology*, 36, 205-213, 1997.

464 Mahesh, A., Eager, R., Campbell, J. R., and Spinhirne, J. D.: Observations of blowing  
465 snow at the South Pole, *Journal of Geophysical Research Atmospheres*, 108, 4707,  
466 2003.

467 Mann, G. W., Anderson, P. S., and Mobbs, S. D.: Profile measurements of blowing  
468 snow at Halley, Antarctica, *Journal of Geophysical Research Atmospheres*, 105,  
469 24491-24508, 2000.

470 Meneveau, C., Lund, T. S., and Cabot, W. H.: A Lagrangian dynamic subgrid-scale  
471 model of turbulence, *Journal of Fluid Mechanics*, 319, 353-385, 1996.

472 Moeng, C. H., and Sullivan, P. P.: A Comparison of Shear- and Buoyancy-Driven  
473 Planetary Boundary Layer Flows, *Journal of the Atmospheric Sciences*, 51,  
474 999-1022, 1994.

475 Mohamed, N., Florence, N. B., and Hugo, M.: Numerical simulation of drifting snow:  
476 erosion and deposition models, *Annals of Glaciology*, 26, 191-196, 1998.

477 Nemoto, M., and Nishimura, K.: Numerical simulation of snow saltation and  
478 suspension in a turbulent boundary layer, *Journal of Geophysical Research*  
479 *Atmospheres*, 109, D18206, 2004.

480 Nishimura, K., and Nemoto, M.: Blowing snow at Mizuho station, Antarctica,  
481 *Philosophical Transactions*, 363, 1647, 2005.

482 Nishimura, K., Yokoyama, C., Ito, Y., Nemoto, M., Naaim - Bouvet, F., Bellot, H.,  
483 and Fujita, K.: Snow particle speeds in drifting snow, *Journal of Geophysical*  
484 *Research Atmospheres*, 119, 9901-9913, 2015.

485 Palm, S. P., Yang, Y., Spinhirne, J. D., and Marshak, A.: Satellite remote sensing of  
486 blowing snow properties over Antarctica, *Journal of Geophysical Research*  
487 *Atmospheres*, 116, D16123, 2011.

488 Pomeroy, J. W., and Essery, R. L. H.: Turbulent fluxes during blowing snow: field  
489 tests of model sublimation predictions, *Hydrological Processes*, 13, 2963-2975,  
490 1999.

491 Pomeroy, J. W., and Gray, D. M.: Saltation of snow, *Water Resources Research*, 26,  
492 1583-1594, 1990.

493 Sbuhei, T.: Characteristics of Drifting Snow at Mizuho Station, Antarctica, *Annals of*  
494 *Glaciology*, 6, 71-75, 1985.

495 Schmidt, R. A.: Vertical profiles of wind speed, snow concentration, and humidity in  
496 blowing snow, *Boundary-Layer Meteorology*, 23, 223-246, 1982.

497 Schmidt, R. A.: Transport rate of drifting snow and the mean wind speed profile,  
498 *Boundary-Layer Meteorology*, 34, 213-241, 1984.

499 Schneiderbauer, S., and Prokop, A.: The atmospheric snow-transport model:  
500 SnowDrift3D, *Journal of Glaciology*, 57, 526-542, 2011.

501 Smagorinsky, J.: GENERAL CIRCULATION EXPERIMENTS WITH THE

502 PRIMITIVE EQUATIONS, Monthly Weather Review, 91, 99-164, 1963.  
503 Sturm, M., and Stuefer, S.: Wind-blown flux rates derived from drifts at arctic snow  
504 fences, Journal of Glaciology, 59, 21-34, 2013.  
505 Sugiura, K., and Maeno, N.: Wind-Tunnel Measurements Of Restitution Coefficients  
506 And Ejection Number Of Snow Particles In Drifting Snow: Determination Of  
507 Splash Functions, Boundary-Layer Meteorology, 95, 123-143, 2000.  
508 Tabler, R. D.: Estimating snow transport from wind speed record : Estimates versus  
509 measurements at Prudhoe Bay, paper presented at Alaska, Meeting of Western  
510 Snow Conference, 1990.  
511 Uematsu, T., Nakata, T., Takeuchi, K., Arisawa, Y., and Kaneda, Y.:  
512 Three-dimensional numerical simulation of snowdrift, Cold Reg.sci.technol, 20,  
513 65-73, 1991.  
514 Vinkovic, I., Aguirre, C., Ayrault, M., and Simoëns, S.: Large-eddy Simulation of the  
515 Dispersion of Solid Particles in a Turbulent Boundary Layer, Boundary-Layer  
516 Meteorology, 121, 283-311, 2006.  
517 Vionnet, V., Martin, E., Masson, V., Guyomarc'H, G., Naaimbouvet, F., Prokop, A.,  
518 Durand, Y., and Lac, C.: Simulation of wind-induced snow transport in alpine  
519 terrain using a fully coupled snowpack/atmosphere model, Cryosphere Discussions,  
520 7, 2191-2245, 2013.  
521 Xue, M., Drogemeier, K. K., Wong, V., Shapiro, A., Brewster, K., Carr, F., Weber, D.,  
522 Liu, Y., and Wang, D.: The Advanced Regional Prediction System (ARPS) – A  
523 multi-scale nonhydrostatic atmospheric simulation and prediction tool. Part II:  
524 Model physics and applications, Meteorology & Atmospheric Physics, 76, 143-165,  
525 2001.  
526 Zhang, J., and Huang, N.: Simulation of Snow Drift and the Effects of Snow Particles  
527 on Wind, Modelling & Simulation in Engineering, 2008, 408075, 2008.  
528 Zwaafink, C. D. G., Diebold, M., Horender, S., Overney, J., Lieberherr, G., Parlange,  
529 M. B., and Lehning, M.: Modelling Small-Scale Drifting Snow with a Lagrangian  
530 Stochastic Model Based on Large-Eddy Simulations, Boundary-Layer Meteorology,  
531 153, 117-139, 2014.